One Novel Soft-Starting Control Strategy for Induction Motor Based on Space Voltage Vectors

Shihong Xie
School of Electrical and Control Engineering
Shaanxi University of Science and Technology
Xi'an China
E-mail: skd2022xin@163.com

Zhihao Yang
School of Electrical and Control Engineering
Shaanxi University of Science and Technology
Xi'an China
E-mail: 1063496939 @qq.com

Rongmao Liang
School of Electrical and Control Engineering
Shaanxi University of Science and Technology
Xi'an China
E-mail: lrmtongxue@163.com

Xin Gao
School of Electrical and Control Engineering
Shaanxi University of Science and Technology
Xi'an China
E-mail: 945788415 @qq.com

Li Liang
School of Electrical and Control Engineering
Shaanxi University of Science and Technology
Xi'an China
E-mail: 3204958360 @qq.com

***Abstract*—This study presents a novel control strategy of discrete variable frequency (DVF) based on space voltage vectors for a three-phase induction motor (IM) soft-starting. The proposed strategy is developed in four steps. First, conducting states of the three-phase thyristor circuits are analysed, and the formation mechanism of space voltage vectors is also demonstrated. Then, DVF control strategy of IM based on hexagon flux linkage loci is expounded categorically, which contains frequency f/7 control, frequency f/4 control, frequency f/3 control and ramp voltage control. Next, under two-phase stationary coordinate system, stator flux equation of IM is derived, and the decrease in stator flux when zero-vector voltage working is calculated accurately. In the end, an experimental system of IM based on three-phase thyristor circuits is constructed, and the experimental results are dealt with and compared with the usual ramp voltage technique. The study results show that IM driven by the proposed strategy can steadily operate at the preset discrete frequency, and the effective value of starting current of IM can be decreased by nineteen percent. The experimental results verify the conclusions.**

Keywords-Induction Motor; Discrete Variable Frequency (DVF); High Starting Torque; Space Voltage Vectors; Thyristor

I. INTRODUCTION

Three-phase induction motors (IMs) are widely utilized in modern industry such as water pumps, draught fans, grinding millers and so on. Large starting currents will damage IM if it is directly started with power supply. So three-phase anti-parallel thyristor circuits based on voltage-regulation technology are often adopted for the soft start of IM [1], which have small starting current. However, using this way, electromagnetic torque of IM has more sacrifice than the decline of its starting current. Though many papers have proposed several methods to enhance start torque of IM, but they are based on constant-current control or closed-torque control [2-3]. [4] and [5] propose a novel control strategy of soft start for IM using pulse width modulation(PWM) AC

DOI: 10.2478/ijanmc-2022-0037

chopper, which uses four insulated gate bipolar transistors(IGBT) to regulate three-phase voltages of IM. This control method is simple and flexible, but the frequency of the three-phase voltages maintains a constant value. The promotion of IM starting torque in papers [2-5] is limited, because these methods all belong to the voltage-regulation control theory of IM.

Based on the three-phase thyristor circuits, Ginart and his cooperators propose a discrete variable frequency (DVF) theory, which can enhance electromagnetic torque of IM with the same starting current [6]. So, DVF theory is welcomed and further investigated in worldwide. In [7], phase control method of DVF optimal switching is studied, which has a favorable effect on solving switch disturbance but don't compare with other methods. In [8-9], one triggering scheme of output equivalent sinusoid voltages based on DVF is proposed, which analyzes the voltage symmetry and acquired available frequency dividing coefficients. It is insufficient that the control method can't consider the flux of IM when two-phase thyristor circuits are triggered. In [10-11], the cause of torque pulsation is studied and the proposed DVF control strategy is based on space voltage vectors, which can decrease the torque pulsation. However, the working principle of space voltage vectors and stator flux of IM isn't analyzed adequately in these papers. In [12] and [13], the causes of electromagnetic torque shocking and rotor speed shocking are analyzed with torque functions and simulation, and the technique used to suppress electromagnetic torque shocking is based on the closed control strategy of power factor angle compensating. While, there are large harmonic components and torque pulses for these DVF control methods proposed in above papers, which are based on periodic wave control theory. So torque increments of these methods are limited. There are other control methods in [14]-[16] based on AC chopper technology for soft-starting of IM, but they are mainly based on regulation voltage theory which can't increase starting torque of IM thoroughly.

In context to insufficient information existing in above the papers, based on [10-11], this paper proposes one novel DVF control strategy of IM based on space voltage vectors, which is realized with three-phase thyristor circuits. This novel control strategy is built on hexagon space voltage vectors and the stator flux linkage loci are controlled directly. Because the frequency of three-phase voltages is reduced with the decline of the effective value of the voltages. So the stator flux and the starting torque of IM driven by the proposed strategy are larger than the ramp voltage control.

II. DVF Principle Based on Space voltage vectors

A. Space voltage vectors based on three-phase thyristor control circuits

According to the principle of space voltage vectors, stator voltage vectors of IM can be written as follows [17].

$$\boldsymbol{u}_s = \sqrt{\frac{2}{3}}(u_{A0}e^{j0} + u_{B0}e^{j2\pi/3} + u_{C0}e^{j4\pi/3}) \qquad (1)$$

Where u_{A0}, u_{B0} and u_{C0} are three-phase stator winding voltages, respectively, and e^{j0}, $e^{j2\pi/3}$ and $e^{j4\pi/3}$ are unit space vector at the directions of A-phase, B-phase and C-phase stator winding axis of IM, respectively.

Thyristor control circuits of IM have three working states, which are two-phase circuits conducting, three-phase circuits conducting and three-phase circuits non-conducting. Space voltage vector will generate when two-phase windings of the IM are supplied with a power source, which are shown as fig.1.

Because stator current of IM will generate when at least two-phase circuits of thyristor control circuits are triggered. So when T1 and T6 are triggered, voltage space vector defined as $\boldsymbol{u}_{AB}$ which is shown in fig. 1(a) will generate in stator winding space of IM. When T1 and T2 are triggered, voltage space vector defined as $\boldsymbol{u}_{AC}$ in fig. 1(b) will generate. Similarly, $\boldsymbol{u}_{BC}$, $\boldsymbol{u}_{BA}$, $\boldsymbol{u}_{CA}$ and $\boldsymbol{u}_{CB}$ are presented in fig. 1(c) to (f). Expressions of following six space voltage vectors are shown here in equations (2) when the initial phase angle of phase-A voltage is equal to zero.

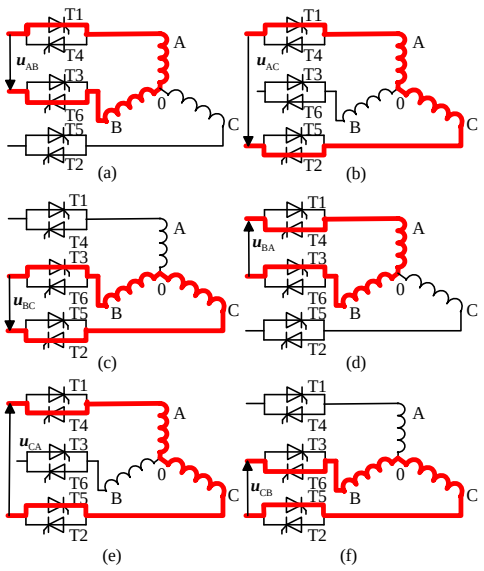

Figure 1. The forming principle of space voltage vectors based on three-phase thyristor circuits. (a) uAB, (b) uAC, (c) uBC, (d) uBA, (e) uCA, (f) uCB.

$$\begin{cases} \boldsymbol{u}_{AB}=\sqrt{\frac{2}{3}}U_m\left(\cos\omega_1 t-\cos(\omega_1 t-\frac{2\pi}{3})e^{\frac{j2\pi}{3}}\right) \\ \boldsymbol{u}_{AC}=\sqrt{\frac{2}{3}}U_m\left(\cos\omega_1 t-\cos(\omega_1 t+\frac{2\pi}{3})\bullet e^{\frac{j4\pi}{3}}\right) \\ \boldsymbol{u}_{BC}=\sqrt{\frac{2}{3}}U_m\left(\cos(\omega_1 t-\frac{2\pi}{3})e^{\frac{j2\pi}{3}}-\cos(\omega_1 t+\frac{2\pi}{3})e^{\frac{j4\pi}{3}}\right) \\ \boldsymbol{u}_{BA}=\sqrt{\frac{2}{3}}U_m\left(\cos(\omega_1 t-\frac{2\pi}{3})e^{\frac{j2\pi}{3}}-\cos(\omega_1 t)\right) \\ \boldsymbol{u}_{CA}=\sqrt{\frac{2}{3}}U_m\left(\cos(\omega_1 t+\frac{2\pi}{3})e^{\frac{j4\pi}{3}}-\cos(\omega_1 t)\right) \\ \boldsymbol{u}_{CB}=\sqrt{\frac{2}{3}}U_m\left(\cos(\omega_1 t+\frac{2\pi}{3})e^{\frac{j4\pi}{3}}-\cos(\omega_1 t-\frac{2\pi}{3})e^{\frac{j2\pi}{3}}\right) \end{cases} \quad (2)$$

Where Um is the peak value of phase voltage, ω1 is the angular frequency of power sources. Meanwhile, the voltage vector that three-phase thyristor circuits are all triggered is defined as $\boldsymbol{u}_{ABC}$. Similarly, the voltage vector with that three-phase thyristor circuits are all closed is defined as $\boldsymbol{u}_0$. According to the actual conducting circuits, $\boldsymbol{u}_{ABC}$ can be compounded with two space voltage vectors in (2).

If the voltage of stator resistance of IM is ignored, the stator flux of IM can be shown as the following [18].

$$\psi=\int(u+R_s\bullet i)dt\approx\int udt \quad (3)$$

Where ψ is the stator flux of IM, u is the stator voltage and R_s is the stator resistance. If the six space voltage vectors shown in (2) are connected in sequence, then one hexagon space voltage vectors will generate and stator flux linkage loci are also one hexagon as in fig.2 shown.

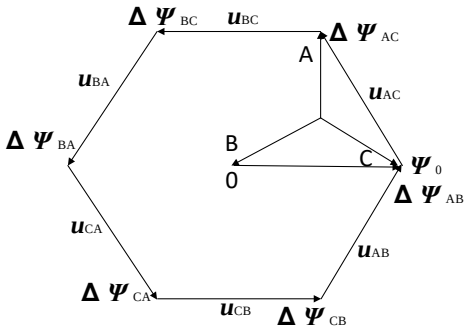

Figure 2. Hexagon space voltage vectors

B. DVF control principle based on space voltage vectors

Depending on the demand of voltage symmetry, the coefficient dividing the frequency of power voltage should be one, four and seven and so on. In case of starting torque of IM, the frequency f/7 can be chosen as the starting frequency of a heavy load IM. Although, the frequency f/3 of voltage doesn't meet the symmetry demand, but its third-harmonic component is a power frequency voltage. So the frequency f/3 of voltage has a good effect on the IM in fact. Therefore, voltage with frequency f/3 can also be utilized to drive an IM. Hence frequency division coefficient of power voltage of DVF would be seven, four, three, and one.

Control methods of DVF frequency f/7 based on space voltage vectors can be realized in following way:

First, based on the zero passage of rising edge of phase-A voltage, T1 and T2 are triggered in order to generate $\boldsymbol{u}_{AC}$, which will trigger angle θ_1. When current i_{AC} declines to zero, T1 and T2 will be closed naturally. Then, during next primitive period of power source, based on the zero passage of falling edge of phase-C voltage, T3 and T2 are triggered in order to generate $\boldsymbol{u}_{BC}$. Their trigger

angles are all θ_2. Circulating this way, after thyristors are closed every time, next vector of hexagonal space voltage vectors will be generated during the next primitive period of the power source. All of hexagonal voltage vectors are generated once during seven primitive periods of the power source. So voltage with frequency f/7 has waves of DVF based on hexagon space voltage vectors is acquired as fig.3 shown.

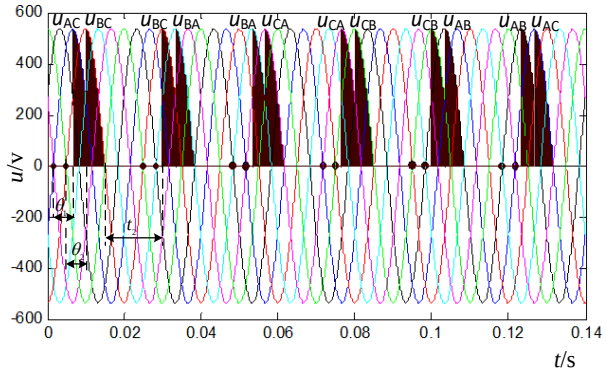

Figure 3. Frequency f/7 voltage waves of DVF based on space voltage vectors

Voltages with frequency f/4 based on three-phase power frequency sinusoid voltages are positive voltages. And control methods of DVF frequency f/4 are also based on hexagonal stator flux linkage loci. But the difference with the control methods of DVF frequency f/7 is that number of working vectors of the former is half of the latter. So voltage with frequency f/4 can be acquired by selectively reducing voltage vectors of frequency f/7 voltage vectors. The sequences of effective voltage vectors are $\boldsymbol{u}_{AC}$ to $\boldsymbol{u}_{BC}$ to $\boldsymbol{u}_{BA}$ to $\boldsymbol{u}_{CA}$ to $\boldsymbol{u}_{CB}$ to $\boldsymbol{u}_{AB}$. The stator flux linkage loci will be three continuous sections which consist of $\boldsymbol{\psi}_{AC}$, $\boldsymbol{\psi}_{BC}$, $\boldsymbol{\psi}_{BA}$, $\boldsymbol{\psi}_{CA}$, $\boldsymbol{\psi}_{CB}$, and $\boldsymbol{\psi}_{AB}$. Frequency f/4 Voltage waveforms are shown in fig.4.

Sequences of effective space voltage vectors of frequency f/3 are $\boldsymbol{u}_{AC}$, $\boldsymbol{u}_{BC}$, $\boldsymbol{u}_{BA}$, $\boldsymbol{u}_{CA}$, $\boldsymbol{u}_{CB}$, and $\boldsymbol{u}_{AB}$, which are also based on hexagonal stator flux linkage loci, but they are divided into two sets. The first set is continuously triggered, containing $\boldsymbol{u}_{AC}$, $\boldsymbol{u}_{BC}$, and $\boldsymbol{u}_{BA}$ while second set is also continuously triggered, which contain $\boldsymbol{u}_{CA}$, $\boldsymbol{u}_{CB}$, and $\boldsymbol{u}_{AB}$. Voltage waveforms of frequency f/3 are shown in fig.5.

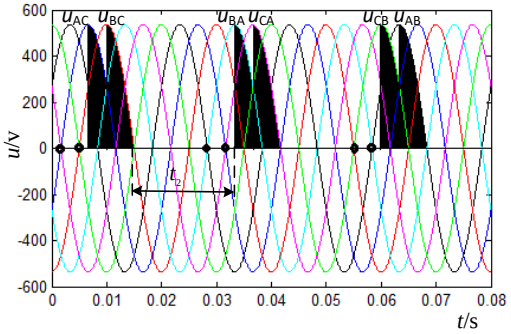

Figure 4. Frequency f/4 voltage waves of DVF based on space voltage vectors

Based on above control methods and space voltage vectors, soft start control of IM is operated in following methods.

Frequency f/7 is selected as the starting frequency of IM. Before soft start, IM is be excited with one voltage vector in several power frequency periods. In order to acquire suitable stator flux, the pre-excited voltage vector will be the previous of the initial voltage vector of frequency f/7, according to the order of hexagon space voltage vectors. For example, if $\boldsymbol{u}_{AC}$ is the first working voltage vector of frequency f/7, then $\boldsymbol{u}_{AB}$ will be the pre-excitation voltage vector. Time for pre-excitation can be calculated by (3) according to the actual IM parameters.

After pre-excitation, IM is driven with the method of DVF having frequency f/7, then frequency f/4, frequency f/3 and frequency f/1 as shown in fig. 3 to 5. Frequency f/1 is the traditional ramp voltage control.

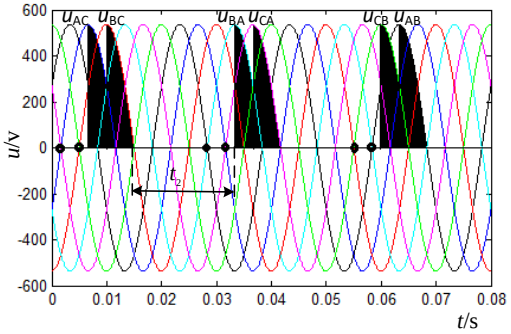

Figure 5. Frequency f/3 voltage waves of DVF based on space voltage vectors

When the working frequency of IM is changed, the previous voltage vector and the next voltage

space vector accord with the sequence of hexagon space voltage vectors as shown in fig. 2. For example, when the working frequency changes from frequency f/7 to frequency f/4, so if $\boldsymbol{u}_{BC}$ is the final voltage vector of frequency f/7 space voltage vectors, then $\boldsymbol{u}_{BA}$ will be the first voltage vector of frequency f/4 voltage vectors. Similarly, when working frequency changes from frequency f/4 to frequency f/3, so if $\boldsymbol{u}_{AB}$ is the final voltage vector of frequency f/4 voltages, then $\boldsymbol{u}_{AC}$ will be the first voltage vector of frequency f/3 voltage vectors. After frequency f/3, IM is controlled by the ramp voltage control.

C. Stator flux analysis of IM

Space voltage vectors of frequency f/3 for IM is used for the stator flux analysis. Stator windings of IM controlled by three-phase thyristor circuits are shown in fig.6. When initial conducting circuits are phase-A and phase-B, and stator windings of IM are star connection, then the current in phase-C stator winding is equal to zero. So phase-C stator winding can be located on α axis of the α-β stationary reference frame, and the equations are acquired as the following.

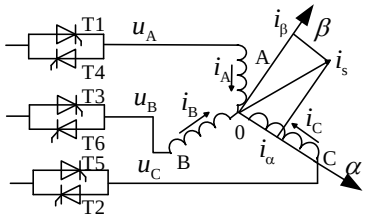

Figure 6. Circuit model of IM under α-β stationary reference frame

$$i_{s\alpha} = 0\ , \quad i_A = -i_B \tag{4}$$

$$i_{s\beta} = \sqrt{\frac{2}{3}}\left(\frac{\sqrt{3}}{2}i_B - \frac{\sqrt{3}}{2}i_A\right) = -\sqrt{2}i_A \tag{5}$$

$$u_{s\beta} = \sqrt{\frac{2}{3}}\left(\frac{\sqrt{3}}{2}u_A - \frac{\sqrt{3}}{2}u_B\right) = \sqrt{2}u_{AB} \tag{6}$$

Where $i_{s\alpha}$ and $i_{s\beta}$ are the α-axis stator current and the β-axis stator current respectively under α-β stationary reference frame, and $u_{s\beta}$ is the stator voltage of α-β stationary reference frame. i_A and i_B are respectively the current in phase-A and phase-B of IM under A-B-C three-phase stationary reference frame. u_{AB} is the line voltage of phase-A to phase-B stator windings. u_{AB} is shown as the following.

$$u_{AB}(t) = \sqrt{3}U_m \sin(\omega_1 t + \alpha_0) \tag{7}$$

Where α_0 is trigger angle of T1 and T6.

Based on the model of IM and from (4) to (7) equations, the following equations are acquired by using Laplace transform.

$$\begin{cases} U_{AB}(s) = -(R_s + sL_s)I_A(s) + \sqrt{2}sL_m I_{r\beta}(s)/2 \\ 0 = (R_r + sL_r)I_{r\alpha}(s) + \omega_r L_r I_{r\beta}(s) - \sqrt{2}\omega_r L_m I_A(s) \\ 0 = (R_r + sL_r)I_{r\beta}(s) - \sqrt{2}sL_m I_A(s) - \omega_r L_r I_{r\alpha}(s) \end{cases} \tag{8}$$

Where L_m is mutual inductance between stator windings and rotor windings, L_s is stator self-inductance, L_r is rotor self-inductance, R_s is stator resistance, R_r is rotor resistance, $I_A(s)$ is the current in phase-A stator winding. $I_{r\alpha}(s)$ and $I_{r\beta}(s)$ are the α axis current and the β axis current of IM under α-β stationary reference frame respectively. ω_r is angular frequency of IM. In order to simplify the progress of solving $I_A(s)$, ω_r is set to be zero. Then IA(s) is solved by using (8).

$$\begin{cases} I_A(s) = P(s)/Q(s) \\ P(s) = \dfrac{\sqrt{3}U_m(-s\cos\alpha_0 + \omega_1 \sin\alpha_0)(1+sT_r)}{R_s T_s T_r'} \\ Q(s) = \left(s^2 + \omega_1^2\right)\left(s^2 + s(\dfrac{1}{T_r'} + \dfrac{1}{T_s'}) + \dfrac{1}{T_s' \bullet T_r'}\right) \end{cases} \tag{9}$$

Where σ=1-L^2_m/(L_sL_r), T_s=L_s/R_s, T_r=L_r/R_r, T'_s=σT_s、T'_r=σT_r. When $Q(s)$ is equal to zero, then there are four roots that can be acquired from the equation. Two of the four roots are complex conjugate: $\lambda_{1,2}$=±jω_1, which correspond to steady components of $I_A(s)$. Another two roots are signed as λ_3 and λ_4. The real parts of λ_3 and λ_4 are negative, which correspond to transient

components of $I_A(s)$. $I_{r\beta}(s)$ are also acquired by using (8).

$$I_{r\beta}(s)=\frac{\sqrt{6}U_m(s\cos\alpha_0-\omega_1\sin\alpha_0)sL_m}{L_sL_r\sigma\left(s^2+\omega_1^2\right)\left(s^2+s(\frac{1}{T_r'}+\frac{1}{T_s'})+\frac{1}{T_s'\bullet T_r'}\right)} \tag{10}$$

Based on the stator flux model of IM: $\boldsymbol{\psi}_s=L_s\boldsymbol{i}_s+L_m\boldsymbol{i}_r$, $\boldsymbol{\psi}_s$ can be calculated by using (4), (5), (8), (9) and (10),

$$\begin{aligned}\boldsymbol{\psi}_s(s)&=j(L_mI_{r\beta}(s)-\sqrt{2}L_sI_A(s))\\&=j\frac{\sqrt{6}U_m(s\cos\alpha_0-\omega_1\sin\alpha_0)\left((1-\sigma+\frac{1}{L_s})s+\frac{1}{L_sT_r}\right)}{\sigma\left(s^2+\omega_1^2\right)\left(s^2+s(\frac{1}{T_r'}+\frac{1}{T_s'})+\frac{1}{T_s'\bullet T_r'}\right)}\end{aligned} \tag{11}$$

Equation (11) can be rewritten by using Laplace inverse transformation as the following.

$$\begin{aligned}\boldsymbol{\psi}_s(t)&=L^{-1}\psi_s(s)\\&=K_1e^{-j\omega_1t}+K_2e^{j\omega_1t}+K_3e^{\lambda_3t}+K_4e^{\lambda_4t}\end{aligned} \tag{12}$$

Where

$$\begin{cases}K_1=\dfrac{\sqrt{6}U_m\omega_1(-\cos\alpha_0+j\sin\alpha_0)\left(-\left(1-\sigma+\frac{1}{L_s}\right)j\omega_1+\frac{1}{L_sT_r}\right)}{\sigma(2j\omega_1)(j\omega_1+\lambda_3)(j\omega_1+\lambda_4)}\\K_2=\dfrac{\sqrt{6}U_m\omega_1(-\cos\alpha_0-j\sin\alpha_0)\left(\left(1-\sigma+\frac{1}{L_s}\right)j\omega_1+\frac{1}{L_sT_r}\right)}{\sigma(2j\omega_1)(j\omega_1-\lambda_3)(j\omega_1-\lambda_4)}\\K_3=\dfrac{j\sqrt{6}U_m(\lambda_3\cos\alpha_0-\omega_1\sin\alpha_0)\left(\left(1-\sigma+\frac{1}{L_s}\right)\lambda_3+\frac{1}{L_sT_r}\right)}{\sigma\left(\lambda_3^2+\omega_1^2\right)(\lambda_3-\lambda_4)}\\K_4=\dfrac{j\sqrt{6}U_m(\lambda_4\cos\alpha_0-\omega_1\sin\alpha_0)\left(\left(1-\sigma+\frac{1}{L_s}\right)\lambda_4+\frac{1}{L_sT_r}\right)}{\sigma\left(\lambda_4^2+\omega_1^2\right)(\lambda_4-\lambda_3)}\end{cases} \tag{13}$$

The stator flux function is acquired by the same method, when $\boldsymbol{u}_{AC}$ and $\boldsymbol{u}_{BC}$ are working. Similarly, $\boldsymbol{u}_0$ is working, then stator current of IM is equal to zero, and the rotor current of IM is shown as following.

$$i_r(t)=i_{r0}e^{-t/T_r} \tag{14}$$

When $\boldsymbol{u}_0$ is working, fig.5 shows that max value of t_3 is 23.3ms and minimum value of t_3 is 13.3ms. When trigger angle becomes equal to ninety degrees, t_3 is 16.7ms. For a common fifteen kilowatt IM, rotor time constant is approximately equal to 300ms which is much larger than t_3. So, based on these parameters and the stator flux model of IM: $\boldsymbol{\psi}_s=L_s\boldsymbol{i}_s+L_m\boldsymbol{i}_r$, stator flux ψ_s can be calculated by using the following equation.

$$\psi_s(t)=L_mi_{r0}e^{-t/T_r}=\psi_0e^{-t/T_r}=0.955\psi_0 \tag{15}$$

Where, ψ_0 is the initial value of ψ_s. Equation (15) shows that the decrement of stator flux is very small and can be neglected when $\boldsymbol{u}_0$ is working.

Using the same method, stator flux can be calculated when IM is also driven by frequency f/7 control method or frequency f/4 control method of DVF.

III. Experiment Validation

A. Simulation

The simulation model is built by Matlab software. Parameters of IM used in the model are shown as the following: P_N=15kW, U_N=380V, n_N=1460r/min, I_N=29.5A, f_N=50Hz, Lm=64.19mH, Rs=0.2147Ω, Rr=0.2205Ω, J=0.602 kg·m^2, $L_{s\sigma}=L_{r\sigma}$=0.991mH. Load rate of IM is 60 percent. Simulation results are shown in fig. 7 to 12.

When IM is driven by control method of DVF with frequency f/7, its line voltage and phase current are shown in fig. 7. The simulation results in fig. 7 show that the period of the line voltage is 0.14ms, and phase current has four continuous conducting sections in time of 0.14ms. So the simulation results in fig.7 verify the principle of control method of DVF with frequency f/7.

Line voltage and phase current of the IM driven by control method of DVF with frequency f/4 are shown in fig 8(a) and fig 8(b) respectively. Fig 8(a) shows that the period of the line voltage is 0.08ms and fig 8(b) shows that phase current has three continuous conducting sections in one frequency f/4 period. The simulation results in fig.8 verify the principle of control method of DVF with frequency f/4.

Similarly, line voltage and phase current for frequency f/3 of DVF are shown in fig. 9. Fig. 9(a) shows that the period of the line voltage is 0.06ms and fig. 9(b) shows that phase current has two continuous conducting sections in time of 0.06ms. The simulation results in fig.9 verify the principle of frequency f/3 control method of DVF.

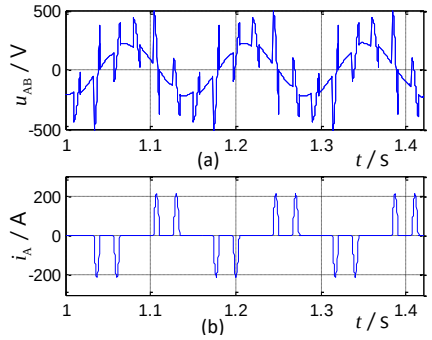

Figure 7. Voltage and current for frequency f/7. (a)Line Voltage. (b) Phase Current.

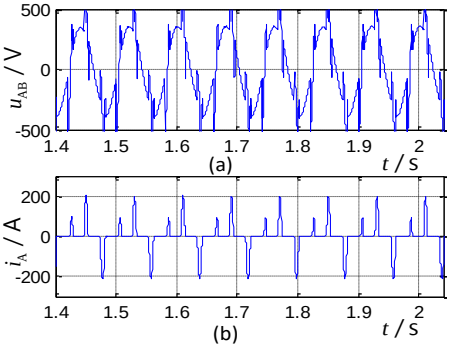

Figure 8. Voltage and current for frequency f/4. (a) Line Voltage. (b) Phase Current.

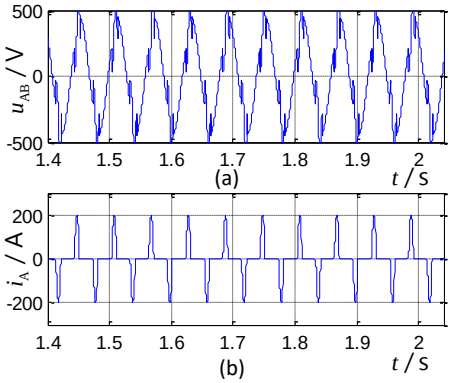

Figure 9. Voltage and current for frequency f/3. (a) Line Voltage. (b) Phase Current.

Stator flux of IM driven by the proposed strategy and the ramp voltage control are shown in fig.10. The results show that the stator flux amplitude of IM driven by the proposed strategy is larger than the flux under the traditional ramp voltage control. The reason is that the frequency of voltage of DVF decreases, but the frequency of voltage of ramp voltage control is a constant value, in the process of soft starting of IM.

Stator current and rotor speed of IM based on the proposed strategy are shown in fig. 11. The result in fig. 11(a) shows that the currents includes four sections which successively corresponded to frequency f/7 current, frequency f/4 current, frequency f/3 current and ramp voltage regulation current. Meanwhile, rotor speed of IM, shown in fig. 11(b), increases accordingly to the proposed control strategy. The simulation results verify the principle of space voltage vectors control of DVF.

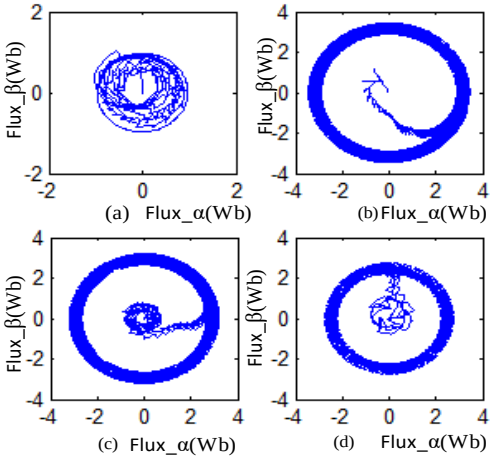

Figure 10. Induction motor stator flux track. (a) ramp voltage. (b) frequency f/7 (c) frequency f/4. (d) frequency f/3.

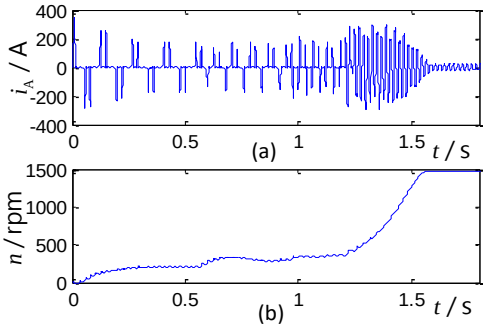

Figure 11. Responses of IM driven by the proposed method. (a) Stator current. (b) Rotor speed.

Contrary to this, stator current and rotor speed of IM driven by ramp voltage control are shown in fig. 12. The results show that rotor speed increases quickly and the value of starting current is very large, which all conform to the principle of ramp voltage soft-starting of IM.

Comparing fig.11 and 12, the current in fig. 11 is smaller than the current in fig. 12, and the rotor speed increases softly. So, the proposed control strategy can acquire better starting performance than ramp voltage control for IM.

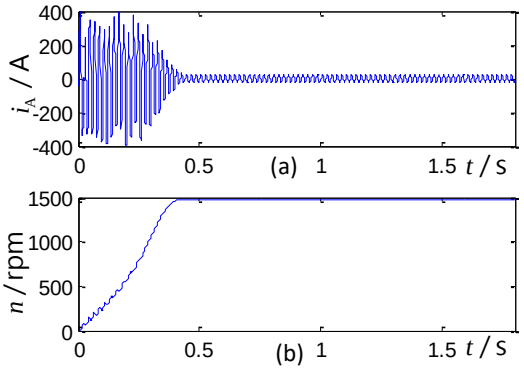

Figure 12. Responses of IM driven by the traditional method. (a) Stator current. (b) Rotor speed.

B. Experiment

For further verifying the performance of the proposed strategy, one experimental set of IM based on three-phase thyristor circuits and STM32F103RC microcontroller is designed as shown in fig. 13. The parameters of IM are same to the parameters used in the simulation model. The experimental results are shown in figs. 14-17.

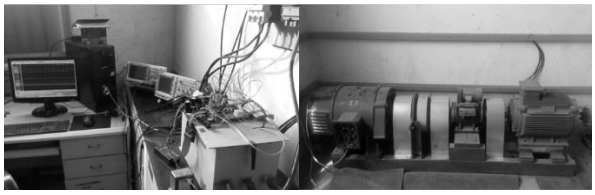

Figure 13. Experimental system of IM driven by three-phase thyristor circuits

Fig. 14 shows the experimental results of IM driven by frequency f/7 of the proposed control strategy. Fig. 14(a) shows the voltage of phase-A to phase-B, while fig. 14(b) shows the current in phase A of IM. They correspond to fig.7 (a) and fig. 7(b) respectively. The experimental results show that the period of the voltage is 0.14ms, and the current has four conducting sections in the period. The experimental results in fig. 14 are in accordance with the simulation results in fig. 7.

Fig. 15 shows the experimental results of IM driven by frequency f/4 of the proposed control strategy. The experimental results in fig. 15 correspond to the simulation results in fig.8. Fig. 15(a) is the voltage of phase-A to phase-B and fig. 15(b) is the current in phase-A of IM. The experimental results show that the period of the voltage is 0.08ms, and the current has three conducting sections in the period. The experimental results in fig.15 are in accordance with the simulation results in fig.8.

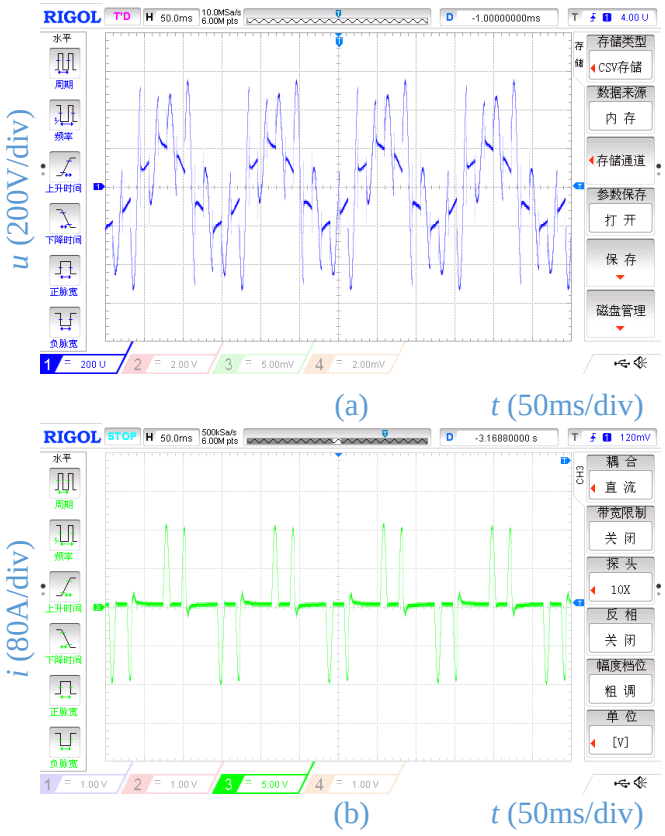

Figure 14. Voltage and current for frequency f/7. (a) Line Voltage (b) Phase Current.

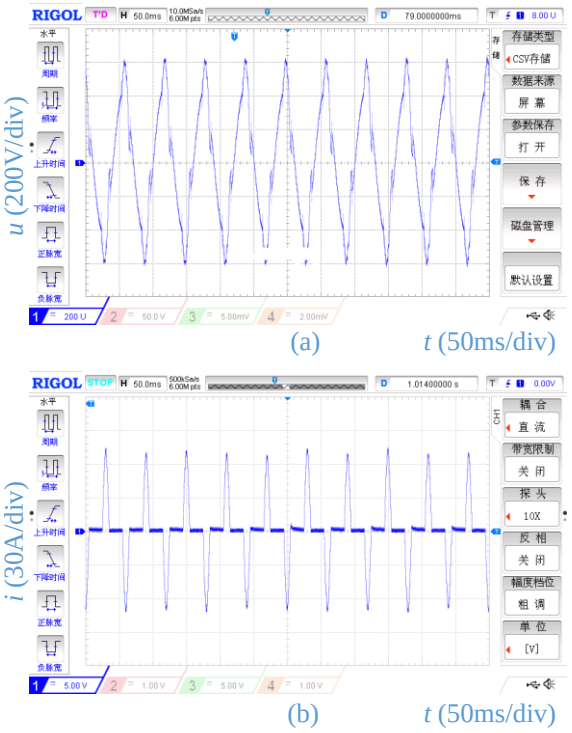

Figure 15. Voltage and current for frequency f/4. (a) Line Voltage. (b) Phase Current.

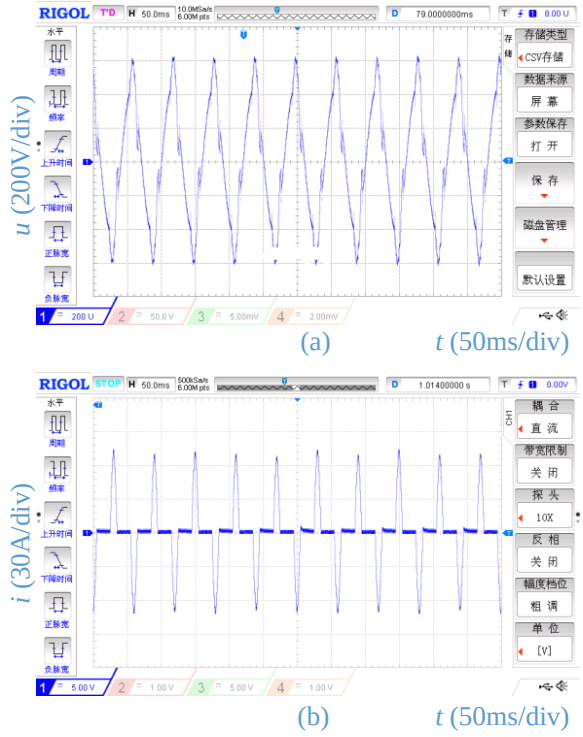

Figure 16. Voltage and current for frequency f/3. (a) Voltage waveform. (b) Current waveform.

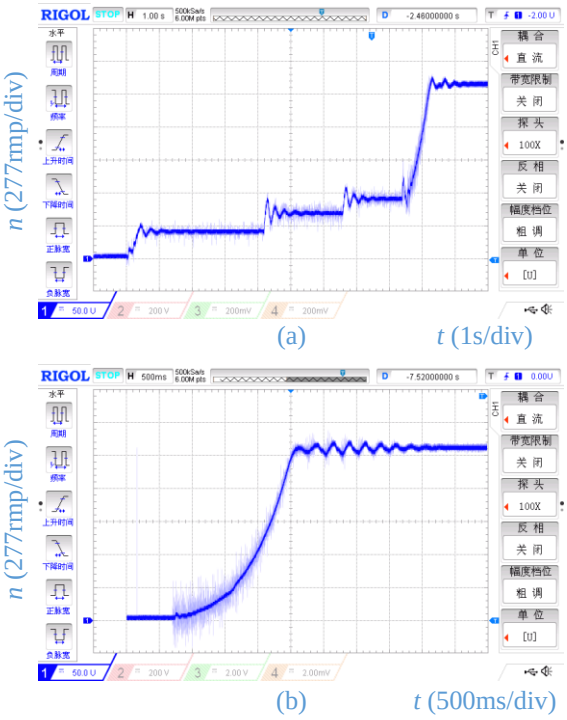

Figure 17. Rotor speeds of IM. (a) The proposed method. (b) The traditional method

Fig.16 shows the experimental results of IM driven by frequency f/3 of the proposed control strategy. The experi-mental results in fig. 16 correspond to the simulation results in fig. 9. Fig. 16(a) is the voltage of phase-A to phase-B and the fig.16 (b) is the current in phase-A of IM. The experimental results show that the period of the voltage is 0. 06ms, and the current has two conducting sections in the period. The experimental results in fig. 16 are in accordance with the simulation results in fig. 9.

Fig.17 demonstrates the rotor speeds of IM driven by the proposed strategy and the traditional ramp voltage. Fig. 17 (a) shows that the rotor speed responds to the proposed strategy. Fig.17 (b) also shows that rotor speed responds to the ramp voltage control. Meanwhile, fig. 17(a) corresponds to the simulation result in fig.11 (b), and fig. 17(b) corresponds to the simulation result in fig.12 (b).

Another experimental results show that the effective value of starting current of IM driven by the proposed strategy with sixty percent load is one hundred and twenty four amperes (124 amps). Whereas when the motor is driven by the ramp voltage control with the same load, the effective

value of starting current is one hundred and fifty four amperes (154 amps). The starting current with the proposed strategy decreases by nineteen percent comparing with the traditional strategy.

IV. CONCLUSION

This paper studies the principle of space voltage vectors based on three-phase thyristor circuits, and proposes the control strategy of DVF based on hexagon space voltage vectors. The study results show that frequency f/7, frequency f/4 and frequency f/3 of power sources can be used to drive IM. The experimental results also show that starting current of a fifteen kilowatt IM driven by the proposed strategy decreases by nineteen percent as comparing to the traditional ramp voltage control with the same load, and rotor speed accurately changes according to the proposed strategy. So, the proposed control strategy of DVF based space voltage vectors is effective for soft starting of IM.

REFERENCES

[1] T.Veera, K.Vijit,K.Anantawat, Comparison of Starting Current Characteristics for Three-Phase nduction Motor Due to Phase-control SoftStarter and Asynchronous PWM AC Chopper," *Journal of Electronical Engineering & Technology*, 2017, Vol.12, No.3, pp. 1090-1100, 2017.

[2] X.Y. Li, J. Xu, H.P, Zhang. "Research on torque ramp current limit starting of induction motor based on dsPIC30F6014," *In Proc. of IEEE Inf. Tech. Net. Elec. Auto. Con.*, pp.1627-1630, Jan. 2018.

[3] A. Nied, J. de Oliveira, R. de F. Campos, et al, "Soft Starting of Induction Motor With Torque Control," *IEEE Trans. Ind. App.*, Vol.46,No.3, pp.1002-1010, 2010.

[4] Said A.D., Haitham Z.A., "Current limiting soft starter for three phase induction motor drive system using PWM AC chopper," IET Power Electronics,Vol.10, No.11, 1298-1306,2017.

[5] Khan, M.M., Rana, A., D., Fei. "Improved ac/ac choppers-based voltage regulator designs," IET Power Electronics, Vol.7, NO. 8, pp.1989-2000, 2014.

[6] A. Ginart, R. Esteller, A Maduro, et al. "High starting torque for AC SCR controller," IEEE Trans Energy Conversion, Vol.14, No.3, pp.553-559, 1999.

[7] F. Zhou, J.L. Cao, J. Liu, et al. "Optimal switching phase and frequency splitting strategy of discrete frequency conversion soft starting control for asynchronous motor," *Electric Machines and Control*, Vol.20,No.3, pp.13-19, 2016.

[8] S.J. Deng, J. Chen, Q. Wang, et al. "A controller of Motor Discrete Variable Frequency Soft Starting and Harmonic Filtering," *2nd Int. Conf. on Sensors, Measurement and Intelligent Materials*, pp.1611-1614, Dec. 2013.

[9] D.H., Li., X.B., Deng. "Research on Discrete Variable Frequency soft starting and electricity-economizing control system of induction motor,"*Int. Conf. Electr. Inf. Control Eng.*, pp. 4391-4394, 2011.

[10] J. Chen, Y.J. Meng, M.L. Duan, et al. "A Starting Method of Induction Motor with High Starting Torque," *Transaction of China Electrotechnical Society*, Vol.32, No.9, pp. 32-39, 2017.

[11] S.H. Xie, Y.J. Meng, J. Chen, et al. "Cause and improvement of the discrete variable frequency torque ripple of induction motor," *Electric Machines and Control*, Vol.22,No.10, pp. 103-111, 2018,.

[12] J. Tong, Z. Zhang, C.Y. Guo, "Study of power factor angle closed-loop control technology in soft-starter," *Electric Machines and Control*, 17, (12), pp. 51-56, 2013.

[13] K.Q. Zhao, D.G. Xu, Y. Wang, "New strategy to improve electromagnetic torque at starting in thyristor controlled induction motors," *The 29th Annual Conference of the IEEE Industrial Electronics Society*, pp.2555-2560, Nov. 2003.

[14] R. L. Gorbunov, G. I. Poskonnyy, "Symmetrical discrete frequency control for AC-chopper with mutual switching function," *International Conference of Young Specialists on Micro/Nanotechnologies and Electron Devices, EDM*, pp. 353-358, Jul. 2014.

[15] K Sundareswaran, P.S R Nayak, "Particle Swarm Optimisation Based Feedback Controller Design for Induction Motor Soft-Starting," *Australian Journal of Electrical and Electronics Engineering*, Vol.11, No.1, pp. 55-63, 2014.

[16] P. Srinivasa Rao Nayak, T.A. Rufzal, "Performance analysis of feedback controller design for induction motor soft-starting using bio-inspired algorithms," *Proc. IEEE Int. Conf. Power, Instrum., Control Comput., PICC*, pp. 1-6, Jun. 2018.

[17] Q.T. An, F. Yao, L.Z. Sun, L. Sun, "SVPWM Strategy of Dual Inverters and Zero-Sequence Voltage Suppression Method," *Proceedings of the CSEE*, Vol.36, No.4, pp. 1042-1049, 2016.

[18] H.Q. Zhang, X.S. Wang, P.F. Wang, et al, "Study on direct torque control algorithm based on space vector modulation," *Electric Machines and Control*, Vol.16, No.6, pp. 13-18, 2012.